SCIENCE CHINA
Information Sciences

• Supplementary File •

Disturbance rejection trajectory tracking control of Mars coaxial rotors UAV via differential flatness

Taiqi WANG[1], Yuanqing XIA[2,1*] & Shunzhi GAO[1]

[1]*School of Automation, Beijing Institute of Technology, Beijing 100081, China*
[2]*Zhongyuan University of Technology, Zhengzhou 450007, China*

Appendix A Mars coaxial rotors UAV modeling

The structure of Mars coaxial rotors UAV is considered as a symmetrical rigid body, and the center of gravity on Mars is coincided with the origin of the body-fixed frame. As depicted in Fig. A1, $\mathcal{F}^m = [x_m, y_m, z_m]$ is the Mars-fixed inertial frame, and $\mathcal{F}^b = [x_b, y_b, z_b]$ is the body-fixed frame. $\xi = [x, y, z]^\top \in \mathbb{R}^3$ is the position vector with respect to the $\mathcal{F}^m$, $\eta = [\phi, \theta, \psi]^\top \in \mathbb{R}^3$ is the attitude angle vector contains three Euler angles, namely roll $\phi \in (-\pi/2, \pi/2)$, pitch $\theta \in (-\pi/2, \pi/2)$ and yaw $\psi \in (-\pi, \pi)$. The coaxial dual-rotor system uses two counter-rotating, vertically stacked rotors of equal diameter and nearly equal speed, producing a total thrust $F_T = F_1 + F_2$, where F_1 and F_2 are the lift forces from the upper and lower rotors, respectively. According to the modeling in [1], the dynamics of the Mars coaxial rotors UAV are described as follows:

$$\begin{cases} \ddot{x} = (cos\psi sin\theta cos\phi + sin\psi sin\phi)u_1 + k_x\dot{x} + d_x, \\ \ddot{y} = (\sin\psi sin\theta cos\phi - \cos\psi sin\phi)u_1 + k_y\dot{y} + d_y, \\ \ddot{z} = -g_m + \cos\theta\cos\phi u_1 + k_z\dot{z} + d_y, \\ \ddot{\phi} = u_2 + k_\phi\dot{\phi}, \\ \ddot{\theta} = u_3 + k_\theta\dot{\theta}, \\ \ddot{\psi} = u_4 + k_\psi\dot{\psi}, \end{cases} \tag{A1}$$

where g_m is the gravity on Mars, d_x, d_y and d_z are the disturbances mainly from wind gusts on Mars, $k_i = K_i/m, i = x, y, z, \phi, \theta, \psi$, where m is the mass, and K_i are the drag coefficients corresponding to different motion models, which must be considered due to the high rotor speeds required in the thin Martian atmosphere. Furthermore, $u_i = U_i/m, i = 1, 2, 3, 4$, are the thrusts during the flight, and $U_1 = F_1 + F_{2z}$ is the collective thrust along the vertical axis, $U_2 = F_{2y}$ and $U_3 = F_{2z}$ are lateral control forces enabling horizontal motion, $U_4 = l_0(F_1 - F_2)$ is provided for the precise yaw control, l_0 is the rotary torque parameters.

Moreover, the dominant external disturbances acting on the Mars coaxial UAV are caused by gusts in the Martian atmosphere. Although gust disturbances may introduce sudden changes in aerodynamic forces, experimental observations and atmospheric models indicate that their magnitudes and rates of variation remain bounded within a finite range. Thus, it is reasonable to assume that the disturbances d_x, d_y, and d_z are continuously differentiable up to the third order.

Appendix B Control objective

The control objective is to drive the Mars coaxial UAV to track the reference trajectory $\xi_r = [x_r, y_r, z_r]^\top$ and desired yaw angle ψ_r under Martian atmospheric conditions. To overcome the inherent underactuation problem, the system is transformed into a fully actuated structure using the differential flatness method. Based on this reformulation, a finite-time disturbance rejection control scheme is developed to ensure precise trajectory tracking. The block diagram is depicted in Fig. B1.

Appendix C Properties analysis of the differential flatness dynamics.

Consider the differential flatness dynamics of the Mars coaxial rotors UAV as follows:

$$\begin{cases} x^{(4)} = (\tau_z + g_m)\tau_1 + 2\dot{\epsilon_1}\dot{\tau}_z + \dfrac{(\ddot{x} - w_x)\ddot{\tau}_z}{\tau_z + g_m} + w_x, \\ y^{(4)} = -(\tau_z + g_m)\tau_2 + 2\dot{\epsilon_2}\dot{\tau}_z - \dfrac{(\ddot{y} - w_y)\ddot{\tau}_z}{\tau_z + g_m} + w_y, \\ \ddot{z} = \tau_z + w_z, \\ \ddot{\psi} = u_4 + k_\psi\dot{\psi}. \end{cases} \tag{C1}$$

* Corresponding author (email: xia_yuanqing@bit.edu.cn)

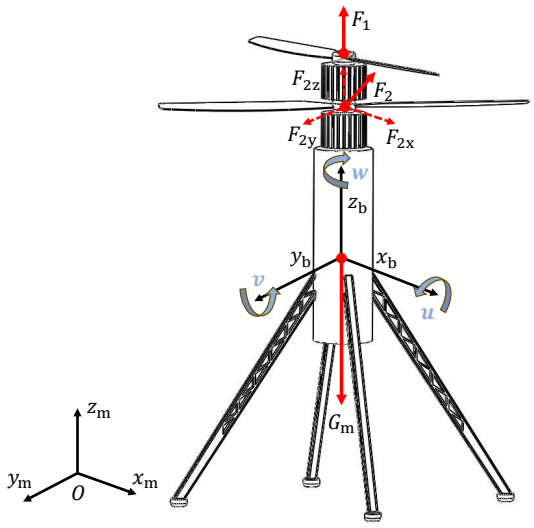

Figure A1 Configuration of the Mars coaxial rotors UAV.

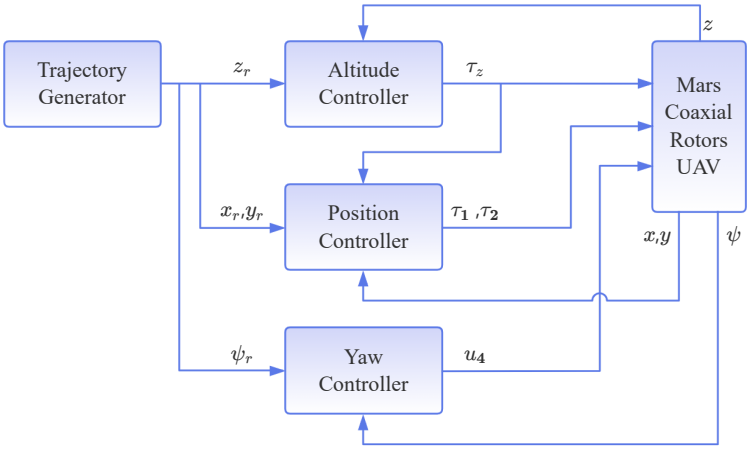

Figure B1 Block diagram of the control system.

Furthermore, ϕ and θ are formulated as

$$\begin{cases} \theta = arctan(\dfrac{(\ddot{x}-w_x)cos\psi + (\ddot{y}-w_y)sin\psi}{\ddot{z}+g_m}), \\ \phi = arcsin(\dfrac{(\ddot{x}-w_x)sin\psi - (\ddot{y}-w_y)cos\psi}{\sqrt{(\ddot{x}-w_x)^2+(\ddot{y}-w_y)^2+(\ddot{z}+g_m)^2}}). \end{cases} \tag{C2}$$

The properties of the differential flatness dynamics are summarized as follows:

• **Flatness and explicit parametrization.** Equations (C2) show that the attitude angles ϕ, θ can be expressed algebraically in terms of the translational accelerations and yaw ψ (and their derivatives appear in (C1)). Therefore, the chosen outputs (x, y, z, ψ) serve as flat outputs: all states and control inputs of the original UAV can be parametrized by these outputs and a finite number of their derivatives. This explicit parametrization greatly simplifies trajectory generation and enables direct computation of required input profiles.

• **Full-actuation in the flat coordinates.** System (C1) has four independent inputs $(\tau_1, \tau_2, \tau_z, u_4)$ and four outputs (x, y, z, ψ), so it is a four-input four-output system. By Definition 1, it is fully actuated in the flat-output coordinates, which removes the original underactuation barrier and permits controller designs that act directly on each output channel.

• **Reduced coupling and increased allocation flexibility.** After flatness-based transformation, the principal coupling between translation and attitude is captured explicitly through the algebraic relations, the terms involving τ_z and its derivatives in (C1). This explicit representation enables more flexible control allocation and reduces the need for implicit compensation of attitude translation coupling in the controller.

• **Robustness and disturbance handling.** Expressing the dynamics in the flat coordinates makes the lumped disturbance terms w_x, w_y, w_z explicit in (C1), which facilitates the design of disturbance observers and disturbance-rejection controllers. The explicit disturbance appearance aids both compensation design and stability analysis.

Appendix D Proof of Theorem 1

To address the stability of the control scheme, two lemmas are given as follows:

Lemma D1. [2] Consider the system $\dot{x} = f(x)$, if there is a Lyapunov function $V(x)$ satisfying $\dot{V}(x) \leqslant -aV(x)^{o_1} - a_1V(x) + bV(x)^{o_2}$, where $a > 0$, $a_1 > 0$, $b > 0$, $0 < o_1 < 1$, and $-\infty < o_2 < o_1$, then the system can achieve finite-time uniformly ultimately bounded (UUB) in a finite time as $T \leqslant \frac{\ln\left[1+(a-\theta_1)^{-1}(a_1-\theta_2)V(x_0)^{1-o_1}\right]}{(a_1-\theta_2)(1-o_1)}$, where $\theta_1 \in (0, a)$, $\theta_2 \in (0, a_1)$.

Lemma D2. [3] For system $\dot{x} = f(x)$, suppose there exists a Lyapunov function $V(x)$ defined on a neighborhood $\mathcal{U} \subset \mathbb{R}^n$ of the origin satisfying $\dot{V}(x) \leqslant -cV(x)^{\mu}$, where $c > 0$ and $0 < \mu < 1$, then x will converge to origin within a finite time as $T \leqslant \frac{V(x_0)^{1-\mu}}{c(1-\mu)}$.

According to the above lemmas, the proof is divided into three parts. First, the finite-time convergence of FESO is analyzed. Then, we verify that the sliding surface enters a small neighborhood within the finite time. Finally, we analyze that the overall system achieves uniform ultimate bounded (UUB) in the finite time.

Part 1: Define $\tilde{p}_i = p_i - \hat{p}_i, i = 1, ..., 5$ as the estimation errors, and denote $\tilde{p} = [\tilde{p}_1, ..., \tilde{p}_5]^\top$, then the estimation error dynamics of FESO can be obtained as

$$\dot{\tilde{p}} = A\tilde{p} + Bh_1(t) - C\lceil\tilde{p}_1\rfloor^{\alpha}, \tag{D1}$$

where

$$A = \begin{bmatrix} -l_{11} & 1 & 0 & 0 & 0 \\ -l_{21} & 0 & 1 & 0 & 0 \\ -l_{31} & 0 & 0 & 1 & 0 \\ -l_{41} & 0 & 0 & 0 & 1 \\ -l_{51} & 0 & 0 & 0 & 0 \end{bmatrix}, B = \begin{bmatrix} 0 \\ 0 \\ 0 \\ 0 \\ 1 \end{bmatrix}, C = \begin{bmatrix} l_{12} \\ l_{22} \\ l_{32} \\ l_{42} \\ l_{52} \end{bmatrix}.$$

Consider the estimation error system (D1), choose the Lyapunov candidate as $V(\tilde{p}) = \tilde{p}^\top Q\tilde{p}$, $Q \in \mathbb{R}^{5\times5}$ is a symmetric positive definite matrix meets $A^\top Q + QA = -I_{5\times5}$. Then we can obtain

$$\begin{aligned} \dot{V}(\tilde{p}) &= \dot{\tilde{p}}^\top Q\tilde{p} + \tilde{p}^\top Q\dot{\tilde{p}} \\ &= \tilde{p}^\top(A^\top Q + QA)\tilde{p} + 2\tilde{p}^\top QBh_1(t) - 2\tilde{p}^\top QC\lceil\tilde{p}_1\rfloor^{\alpha}. \end{aligned} \tag{D2}$$

According to the results in [2], there exist proper positive parameters a_1, a_2 and a_3, such that

$$\dot{V}(\tilde{p}) \leqslant -a_1V(\tilde{p})^{\frac{1+\alpha}{2}} - a_2V(\tilde{p}) + a_3V(\tilde{p})^{\frac{1}{2}}. \tag{D3}$$

According to Lemma D1, the estimation errors will achieve finite-time convergence in a bounded time t_1, which can be obtained as $t_1 \leqslant \frac{\ln\left[1+(a_1-\chi_1)^{-1}(a_2-\chi_2)V(x_0)^{\frac{1-\alpha}{2}}\right]}{(a_2-\chi_2)^{\frac{1-\alpha}{2}}}$, where $\chi_1 \in (0, a_1)$, $\chi_2 \in (0, a_2)$.

Part 2: Consider the sliding variable, define the Lyapunov function as $V(s_1) = \frac{1}{2}s_1^\top s_1$, it follows from the results of $\dot{V}_4$ that $\dot{V}(s_1) \leqslant -k_{s_1}\|s_1\|^{\gamma+1} + \|s_1\| \cdot \|\tilde{p}_5\|$. When $t \to t_1$, it can be approximated that $\|\tilde{p}_5\| \to 0$, thus $\dot{V}(s_1) \leqslant -k_{s_1}(2V(s_1))^{\frac{\gamma+1}{2}}$ as $t > t_1$. Based on Lemma D2, s_1 can achieve finite-time convergence in a bounded time as $t_2 \leqslant \frac{2V(s_1(0))^{(1-\gamma/2)}}{(1-\gamma)2^{(1+\gamma/2)}k_{s_1}}$.

Part 3: Consider the system (6) under controller (12), choose the Lyapunov function as $V_5 = \sum_{i=1}^{4} \mathrm{V}_i$. It follows from (9)–(12) that $\dot{V}_5 \leqslant -k_{s_1}\|s_1\|^{\gamma+1} + \|s_1\| \cdot \|\tilde{p}_5\|$. According to the above conclusions, estimation errors can achieve finite-time convergence in t_1, and s_1 can achieve finite-time convergence in t_2, thus the system can be guaranteed to be UUB as $t > \frac{\ln\left[1+(a_1-\chi_1)^{-1}(a_2-\chi_2)V(x_0)^{\frac{1-\alpha}{2}}\right]}{(a_2-\chi_2)^{\frac{1-\alpha}{2}}}$, where $\chi_1 \in (0, a_1)$, $\chi_2 \in (0, a_2)$. The proof is completed.

Appendix E Altitude Controller Design

Consider the altitude dynamics in (5), denote $v_z = \dot{z}$, one can obtain

$$\begin{cases} \dot{z} = v_z, \\ \dot{v}_z = \tau_z + w_z. \end{cases} \tag{E1}$$

Denote $z_1 = z$, $z_2 = v_z$, $z_3 = w_z$ as the extended state, and $\dot{z}_3 = h_2(t)$ is bounded, then the FESO is given as follows:

$$\begin{cases} \dot{\hat{z}}_1 = \hat{z}_2 + l_{z1}\tilde{z}_1 + l_{z2}\lceil\tilde{z}_1\rfloor^{\alpha_z}, \\ \dot{\hat{z}}_2 = \hat{z}_3 + l_{z3}\tilde{z}_1 + l_{z4}\lceil\tilde{z}_1\rfloor^{\alpha_z} + \tau_z, \\ \dot{\hat{z}}_3 = l_{z5}\tilde{z}_1 + l_{z6}\lceil\tilde{z}_1\rfloor^{\alpha_z}, \end{cases} \tag{E2}$$

where $\hat{z}_i, i = 1, 2, 3$, are the estimates of z_i, $\tilde{z}_i = z_i - \hat{z}_i$ are the estimation errors. $l_{zi}, i = 1, .., 6$ are positive parameters, $\alpha_z \in (0, 1)$. Denote $\tilde{z} = [\tilde{z}_1, \tilde{z}_2, \tilde{z}_3]^\top$, then the estimation error dynamics can be formulated as

$$\dot{\tilde{z}} = A_z \tilde{z} + B_z h_2(t) - C_z \lceil \tilde{z}_1 \rfloor^{\alpha_z}, \tag{E3}$$

where

$$A_z = \begin{bmatrix} -l_{z1} & 1 & 0 \\ -l_{z3} & 0 & 1 \\ -l_{z5} & 0 & 0 \end{bmatrix}, B_z = \begin{bmatrix} 0 \\ 0 \\ 1 \end{bmatrix}, C_z = \begin{bmatrix} l_{z2} \\ l_{z4} \\ l_{z6} \end{bmatrix}.$$

Consider the backstepping controller design, denote the tracking error $e_{z1} = z_r - z_1$, thus $\dot{e}_{z1} = \dot{z}_r - z_2$. Define the virtual controller as $\alpha_{z1} = c_{z1} e_{z1} + \dot{z}_r$, where c_{z1} is a positive parameter, then we define $e_{z2} = \alpha_{z1} - z_2$, thus we have $\dot{e}_{z2} = c_{z1} \dot{e}_{z1} + \ddot{z}_r - z_2$. Combine the above results, we can obtain that $\dot{e}_{z1} = -c_{z1} e_{z1} + e_{z2}$, and $\dot{e}_{z2} = c_{z1}(-c_{z1} e_{z1} + e_{z2}) + \ddot{z}_r - \tau_z - w_z$. As a result, the controller is designed as

$$\tau_z = (1 - c_{z_1}^2) e_{z1} + (c_{z1} + k_z) e_{z2} + k_{sz} \lceil s_z \rfloor^{\gamma_z} - \hat{z}_3 + \ddot{z}_r, \tag{E4}$$

where k_z, k_{s_z}, $\gamma_z \in (0, 1)$ are positive constants, and the sliding mode is $s_z = e_{z2}$.

Theorem E1. Consider the system (E1) under the FESO (E2) and the controller (E4), if $\|h_2(t)\|$ is bounded, then the sliding variable s_z will enter into a small region in finite time, and the system can achieve boundness after the finite time.

Proof. The proof follows a similar procedure to the position controller and is omitted here for brevity.

Appendix F Yaw Angle Controller Design

Consider the yaw dynamics in (5), define tracking error as $e_{\psi_1} = \psi_r - \psi$ and the virtual controller as $\alpha_{\psi_1} = c_{\psi_1} e_{\psi_1} + \dot{\psi}_r$, where c_{ψ_1} is a positive parameter. Then define the yaw angular speed tracking error as $e_{\psi_2} = \alpha_{\psi_1} - \dot{\psi}$, then its derivative is given by $\dot{e}_{\psi_2} = -c_{\psi_2} e_{\psi_2} - e_{\psi_1}$, where $c_{\psi_2} > 0$ is a constant. Based on the above results, the yaw angle controller is designed as

$$\begin{aligned} u_4 = {} & (1 - c_{\psi_1}^2) e_{\psi_1} + (c_{\psi_1} + c_{\psi_2}) e_{\psi_2} \\ & + k_{s\psi} \lceil s_\psi \rfloor^{\gamma_\psi} - k_\psi \dot{\psi} + \ddot{\psi}_r, \end{aligned} \tag{F1}$$

where k_{s_ψ}, $\gamma_\psi \in (0, 1)$ are positive constants, and the sliding mode is $s_\psi = e_{\psi_2}$.

Similar to the analysis of the position controller, it can be concluded that, under the action of controller (E4), the yaw angle tracking error can achieve UUB within a finite time.

Appendix G Extension to higher-order systems

Consider a general nth-order single-input system of the form

$$\dot{x}_i = x_{i+1}, \quad i = 1, \ldots, n-1, \qquad \dot{x}_n = u + d(t), \tag{G1}$$

where x_i represents the state variables, u is the control input, and $d(t)$ denotes the external disturbance.

For such a system, an $(n+1)$-order finite-time extended state observer (FESO) can be constructed in a form analogous to the fourth-order observer proposed in this paper. By following the same finite-time stability analysis framework, it can be shown that the estimation error of the $(n+1)$-order FESO converges to a neighborhood of the origin within finite time.

Based on the observer estimates, a backstepping-based disturbance rejection controller can be designed to stabilize the nth-order system. The recursive backstepping structure allows the control law to be systematically extended to higher-order dynamics without altering the underlying control architecture. Furthermore, the closed-loop stability can be guaranteed using similar finite-time Lyapunov analysis as in the lower-order case.

This indicates that the proposed control framework is not restricted to second- or fourth-order translational dynamics but is inherently applicable to more general high-order systems, thereby enhancing its scalability and adaptability under disturbance conditions.

Appendix H Simulations Results

Appendix H.1 Parameters tuning

Consider the position control part, the tuning process of the finite-time extended state observer (FESO) and backstepping controller are given as follows.

(1) FESO: We first neglect the nonlinear terms and focus on the linearized dynamics to determine the observer bandwidth ω. A suitable bandwidth is selected based on the trade-off between estimation speed and noise sensitivity. Once ω_1 is fixed, the linear gains are chosen according to the standard bandwidth-based tuning rule:

$$l_{11} = 5\omega_1, \quad l_{21} = 10\omega_1^2, \quad l_{31} = 10\omega_1^3, \quad l_{41} = 5\omega_1^4, \quad l_{51} = \omega_1^5. \tag{H1}$$

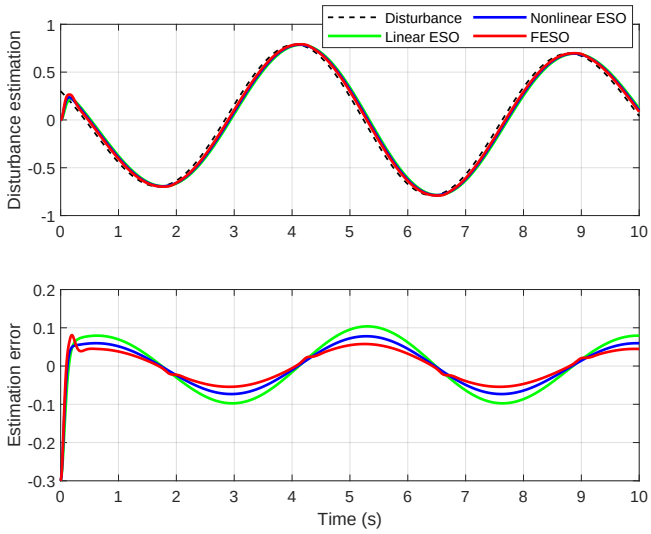

Figure H1 Disturbance estimation results.

After the linear gains are determined, we fine-tune the nonlinear gains l_{i2} $(i = 1, \ldots, 5)$ and the exponent parameter α in the finite-time terms. The tuning is performed iteratively to achieve a balance between fast convergence and noise robustness. The main principle is to increase l_{i2} moderately to enhance convergence speed, while ensuring that the observer does not amplify high-frequency noise.

(2) Backstepping controller: For the backstepping controller, the tuning process is performed in two main steps. First, the parameters c_1, c_2, and c_3 are tuned to determine the controller gains k_i $(i = 1, \ldots, 4)$. These parameters are selected to ensure stable closed-loop performance and satisfactory transient behavior. Next, k_5 and γ $(0 < \gamma < 1)$ are fine-tuned to further improve convergence speed and disturbance rejection capability, while avoiding excessive control effort.

The tuning procedures for the altitude controller and the yaw angle controller follow a similar process. It should be noted that for the FESO in the z-channel, parameters adjustment for the linear gains also follows the bandwidth-based tuning rule, namely selecting ω_2, then $l_{z1} = 5\omega_2, l_{z3} = 10\omega_2^2, l_{z5} = 10\omega_2^3$.

Appendix H.2 Comparison results of ESO

To validate the effectiveness of FESO, we consider the system as $\dot{x}_1 = x_2, \dot{x}_2 = u + d(t)$, where $d(t)$ is the disturbance. Let $x_3 = d(t)$,then we design the FESO as

$$\begin{cases} \dot{\hat{x}}_1 = \hat{x}_2 + l_1\tilde{x}_1 + l_2\lceil\tilde{x}_1\rfloor^{\alpha_0}, \\ \dot{\hat{x}}_2 = \hat{x}_3 + l_3\tilde{x}_1 + l_4\lceil\tilde{x}_1\rfloor^{\alpha_0} + u, \\ \dot{\hat{x}}_3 = l_5\tilde{x}_1 + l_6\lceil\tilde{x}_1\rfloor^{\alpha_0}, \end{cases} \tag{H2}$$

where $\hat{x}_i, i = 1, 2, 3$, are the estimates of $x_i, i = 1, 2, 3$, $l_j, j = 1, ..., 6$, $\alpha_0 \in (0, 1)$ are the positive parameters, $\tilde{x}_1 = x_1 - \hat{x}_1$. Denote $d(t) = 0.3cos(1.5t) - 0.5sin(1.2t)$, $a = 60, l_1 = 3a, l_3 = 3a^2, l_5 = a^3, l_2 = 1, l_4 = 3, l_6 = 5, \alpha_0 = 0.5$. We compared the fine tuning results of the traditional linear ESO with the nonlinear ESO of equation (2.16) in [4], the results are shown in Fig H1. It can be seen that our FESO exhibits a smaller convergence error compared to the traditional ESOs.

Appendix H.3 Complex trajectory tracking

In this section, a set of trajectory tracking simulation is performed to validate the effectiveness of the proposed method.

First, the parameters of the Mars UAV are given in Table H1. We set the bandwidth as $\omega_1 = \omega_2 = 5$, then the parameters of position controller, altitude controller, and yaw angle controller are given in Tables H2–H4, respectively.

Then, the reference trajectory (unit:m) of the Mars UAV from takeoff, through the execution of the flight mission, to landing is given as follows.

$$x_r(t) = \begin{cases} 3\cos(0.4t), & 0 \leqslant t \leqslant 4\pi \\ 3, & 4\pi < t \leqslant 20 \\ 0.7(t-20)+3, & 20 < t \leqslant 30 \\ 10, & 30 < t \leqslant 40 \\ 10 - 10S(\tau), & 40 < t \leqslant 50 \end{cases}, \quad y_r(t) = \begin{cases} 3\sin(0.4t), & 0 \leqslant t \leqslant 4\pi \\ 0.3(t-4\pi), & 4\pi < t \leqslant 20 \\ 3, & 20 < t \leqslant 30 \\ 3 - 0.3(t-30), & 30 < t \leqslant 40 \\ 0, & 40 < t \leqslant 50 \end{cases},$$

$$z_r(t) = \begin{cases} 0.25t + 1, & 0 \leqslant t \leqslant 4\pi \\ 0.25 \times 4\pi + 1, & 4\pi < t \leqslant 40 \\ 4.1416 - 3.1416S(\tau), & 40 < t \leqslant 50 \end{cases}$$

Table H1 Mars UAV parameters

Mass and gravity			Inertia		
m	1.8	kg	I_x	0.004	kg·m^2
g_m	3.71	m/s^2	I_y	0.004	kg·m^2
			I_z	0.009	kg·m^2
Translational damping			Rotational damping		
k_x	0.1		k_ϕ	0.05	
k_y	0.1		k_θ	0.05	
k_z	0.1		k_ψ	0.05	

Table H2 Position controller parameters for the Mars UAV

	ESO gains										
Parameters	l_{11}	l_{21}	l_{31}	l_{41}	l_{51}	l_{12}	l_{22}	l_{32}	l_{42}	l_{52}	α
Values	25	250	1250	2500	3125	1.5	2.5	3.5	4.5	5.5	0.5
	Controller parameters										
Parameters	c_1	c_2	c_3	k_5	k_s	γ					
Values	0.5	1.0	2.0	5	5	0.6					

Table H3 Altitude controller parameters for the Mars UAV

	ESO gains						
Parameters	l_{z1}	l_{z3}	l_{z5}	l_{z2}	l_{z4}	l_{z6}	α_z
Values	25	250	1250	1.5	2.5	3.5	0.5
	Controller parameters						
Parameters	c_{z1}	k_z	k_{sz}	γ_z			
Values	2.0	5	2	0.5			

Table H4 Yaw controller parameters for the Mars UAV

	Controller parameters			
Parameters	$c_{\psi 1}$	$c_{\psi 2}$	$k_{s\psi}$	γ_ψ
Values	0.5	1.0	0.1	0.1

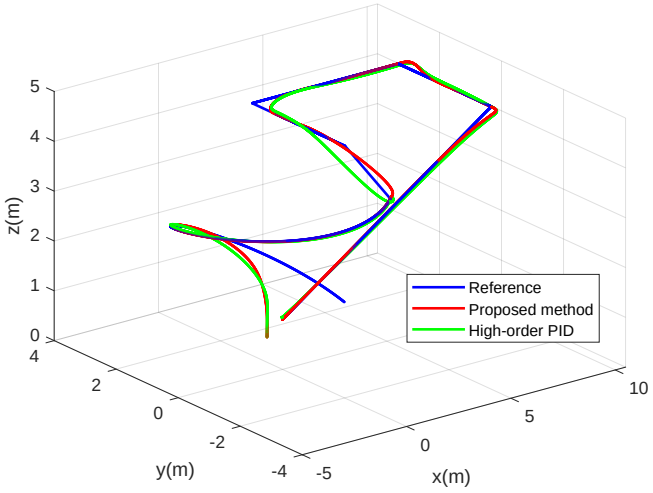

Figure H2 Trajectory tracking results in 3D environment.

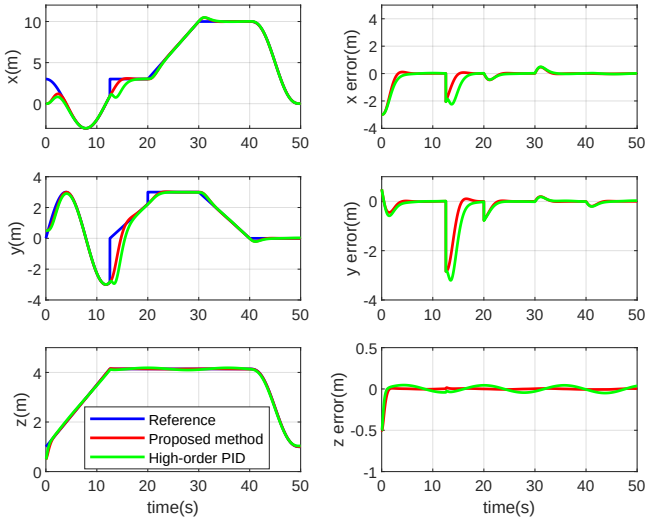

Figure H3 Trajectory tracking results in three directions.

where the smooth S-curve function is defined as:

$$S(\tau) = 10\tau^3 - 15\tau^4 + 6\tau^5, \quad \tau = \min\left(\frac{t-40}{T_f}, 1\right), \quad T_f = 10\,\text{s}.$$

To emulate gust disturbances acting on the UAV in the Martian atmosphere, the perturbations are imposed along each axis, modeled as $d_x = 2\sin(0.6t)$ for the x-axis, $d_y = 2\sin(0.5t)$ for the y-axis, and $d_z = 2\sin(0.4t)$ for the z-axis. Fig H2 illustrates the complete trajectory tracking process of the Mars UAV. The flight begins with a spiral ascent during takeoff, followed by a step-like maneuver to reach a new position, then transitions into horizontal flight, and finally returns to the vicinity of the takeoff point at an altitude of $1m$. Fig H3 presents the trajectory tracking performance along the three spatial directions. It can be observed that under gust disturbances in the Martian atmosphere, the proposed method achieves not only higher tracking accuracy but also faster error convergence compared to the high-order PID controller. Fig H4 shows that during the flight, the attitude angles remain bounded within a safe range, thereby ensuring the stable and safe operation of Mars UAV. Fig H5 illustrates that the control inputs exhibit larger variations during certain critical flight phases but remain within a reasonable range during steady flight. Consequently, the above results confirm that the proposed control strategy ensures precise trajectory tracking, stable attitude regulation, and reasonable control effort under Martian gust disturbances.

Appendix H.4 Parameters sensitivity analysis

In this subsection, we investigate the sensitivity of the system to parameter variations. Since the ψ channel involves relatively few design parameters, our analysis primarily focuses on the x, y, and z channels, which are susceptible to external disturbances. We ensure that all conditions remain consistent with Appendix H.3, and define the integral of

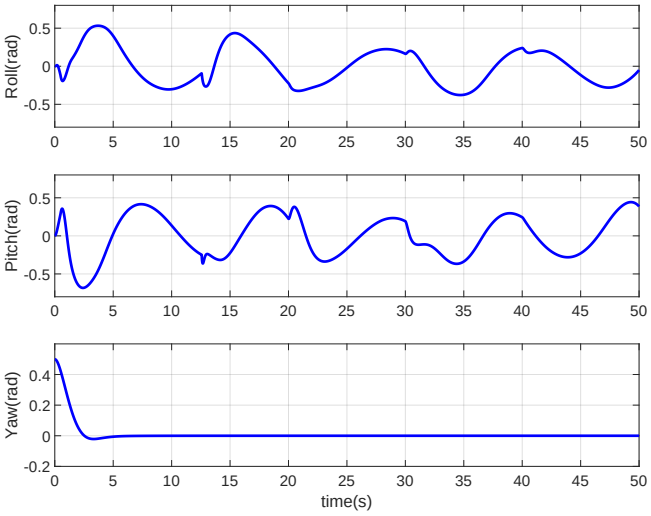

Figure H4 Attitude angles of Mars UAV.

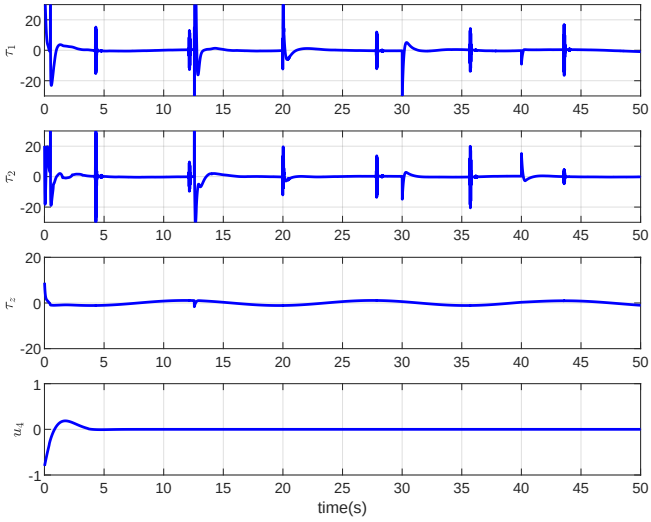

Figure H5 The control inputs of fully actuated system.

absolute error (IAE), which is described as IAE $= \int_{t=0}^{T} (|e_x| + |e_y| + |e_z|)d\tau$ (unit: $m \cdot s$) as the comparison criteria of the experiments, where T is the experiment execution time, e_x, e_y, and e_z are the tracking errors in three directions. The parameter sensitivity analysis is conducted as follows.

First, the impact of parameters involved in FESO is investigated. We select $\omega_i, i = 1, 2$, $l_{j2}, j = 1, ...5$, $l_{zk}, k = 2, 4, 6$, as representative parameters for analysis, while keeping all controller parameters unchanged. Since variations in the FESO parameters have relatively minor effects on the overall control system performance, we adjust them by increasing and decreasing their nominal values by 40% to provide a clearer comparison. The results are shown in Table. H5. The comparison results show that when the parameters are either increased or decreased within the selected range, the control accuracy exhibits a degradation.

Table H5 Parameters analysis of FESO

Parameters of FESO	**IAE** $(\mathrm{m} \cdot \mathrm{s})$
$\omega_i,\ l_{j2},\ l_{zk}$	17.4885
$0.6\omega_i,\ 0.6l_{j2},\ 0.6l_{zk}$	17.5807
$1.4\omega_i,\ 1.4l_{j2},\ 1.4l_{zk}$	17.5697

Second, the impact of parameters related to controllers is investigated. We select $c_i, i = 1, 2, 3$, k_5, k_s, c_{z1}, k_z, and k_{sz} as representative parameters for analysis, while keeping all the parameters of FESO unchanged. Since variations of the controller parameters have relatively major effects on the overall control system performance, we adjust them by increasing

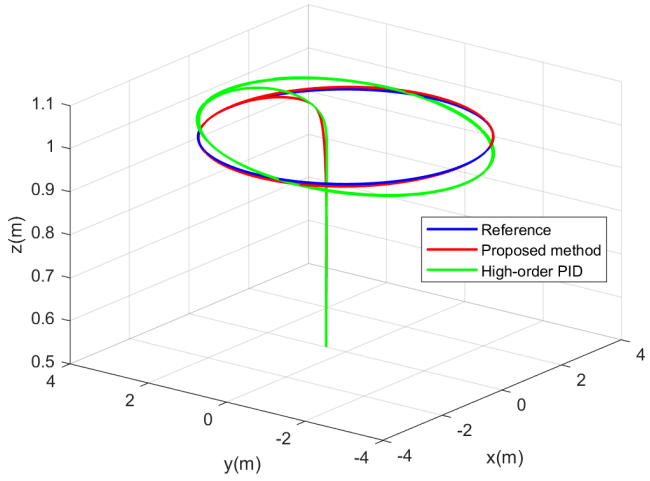

Figure H6 Circle-shape trajectory tracking results in 3D environment.

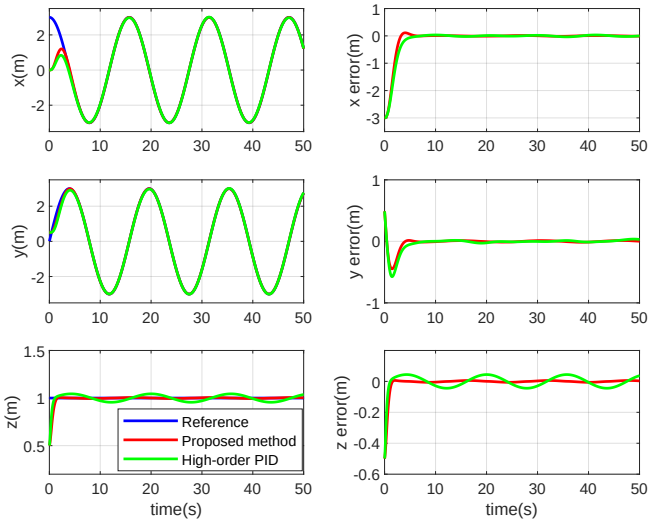

Figure H7 Circle-shape trajectory tracking results in three directions.

and decreasing their nominal values by 20% to provide comparisons. The results are shown in Table. H6. As shown in Table. H6, increasing the parameter values can improve control accuracy. However, the validation results indicate that higher parameter values are accompanied by the increase in control input magnitude, which poses a significant challenge to the control safety of Mars UAVs. Therefore, it is necessary to strike a balance between control accuracy and control input amplitude, ensuring that control performance is maintained while keeping the control inputs within a safe range.

Table H6 Parameters analysis of the controller

Parameters of controller	**IAE** $(\mathrm{m}\cdot\mathrm{s})$
$c_i,\ k_5,\ k_s,\ c_{z1},\ k_z,\ k_{sz}$	17.4885
$0.8c_i,\ 0.8k_5,\ 0.8k_s,\ 0.8c_{z1},\ 0.8k_z,\ 0.8k_{sz}$	30.9789
$1.2c_i,\ 1.2k_5,\ 1.2k_s,\ 1.2c_{z1},\ 1.2k_z,\ 1.2k_{sz}$	15.1056

Appendix H.5 Circle trajectory tracking

In this subsection, to simulate the Mars UAV conducting inspection tasks after ascending to a certain altitude, we have specified the desired trajectory as: $x_r = 3\cos(0.4t)m, y_r = 3\sin(0.4t)m, z_r = 1m$. The parameters remain consistent with the previous subsection. We add the same disturbances as in the previous subsection. The results are depicted in Figs. H6–H9. It can be seen that, under this scenario, the proposed control architecture enables the full-actuated system to achieve higher trajectory tracking accuracy while keeping the attitude angles and control inputs within certain ranges.

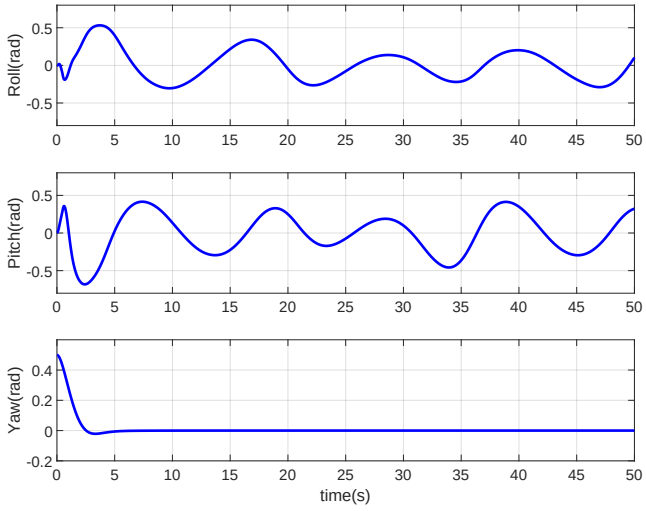

Figure H8 Attitude angles under circle-shape trajectory tracking.

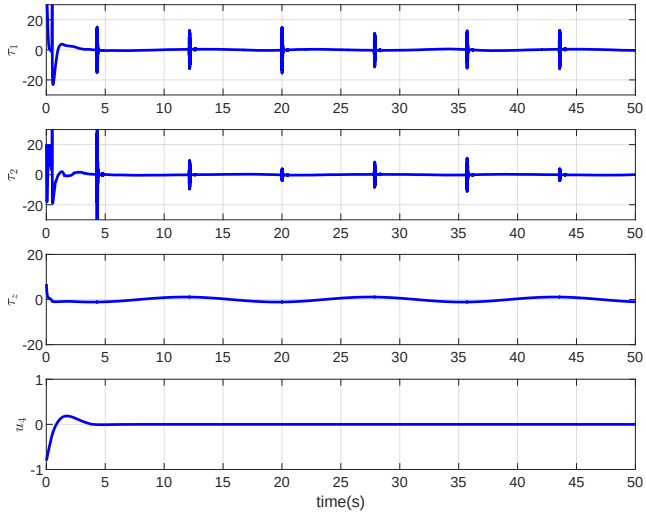

Figure H9 The control inputs under circle-shape trajectory tracking.

References

1 Wei Y, Deng H, Pan Z, et al. Research on a combinatorial control method for coaxial rotor aircraft based on sliding mode. Defence Technol, 2022, 18: 280C292.
2 Gu S, Zhang J, Lin X, et al. Finite-time variable-gain ADRC for masterCslave teleoperated parallel manipulators. IEEE Trans Ind Electron, 2023, 71: 9234C9243.
3 Li Z, Ji H, Finite-time consensus and tracking control of a class of nonlinear multiagent systems. IEEE Trans Autom Control, 2018, 63: 4413C4420.
4 Guo B Z, Zhao Z L, On the convergence of an extended state observer for nonlinear systems with uncertainty. Syst Control Lett, 2011, 60: 420C430.